

A Compact 45 V-to-54 kV Modular DC-DC Converter

Sanghyeon Park, Lei Gu, and Juan Rivas-Davila

Department of Electrical Engineering

Stanford University

Stanford, CA 94305

Email: spark15@stanford.edu

Abstract—This paper presents the design of a compact 45 V-to-54 kV dc-dc converter for high-energy beam applications with the focus on X-ray generation. We describe key design choices for a high power density including a modular structure, high-frequency switching, planar transformers and Dickson topology. High-voltage insulation and thermal management are also described in detail. The experimental data with a 5 kV single module and a 10-module 54 kV converter indicate that the proposed structure can generate high dc voltage while achieving a several times higher power density compared to commercial high-voltage power supplies.

I. INTRODUCTION

High-energy beams such as X-ray or neutron beams are important in many medical, industrial, and security applications. To generate a high-energy beam, a power supply is needed that provides a voltage in the range of 50-200 kV and a current in the range of a few to tens of mA. Developing a compact high-voltage power supply will thus open up a way to realize portable high-performance X-ray imaging devices [1], CT scanners, or neutron scanners to find an oil well [2] or detect nuclear materials in a cargo [3].

In this paper, we first present a 45 V-to-5 kV, 100 W power converter. The power density is 695 W/dm³ (11.4 W/in³), the efficiency is 77 %, and the specific power is 0.636 W/g. The low input voltage makes it easy to power the circuit with a battery for portable applications. The input-to-output isolation isolation capacity is 55 kV_{dc}, making the circuit suitable for parallel-input series-output configuration. We then demonstrate a 45 V-to-54 kV dc-dc power converter by stacking ten of the 5 kV module while maintaining the same efficiency, power density, and specific power as the single module.

II. ISOLATED 45 V-TO-5 KV CIRCUIT DESIGN

A. Power Processing Stage

1) *Choice of the Input and Output Voltages*: Fig. 1 shows the schematic and the implementation of the 45 V-to-5 kV isolated dc-dc converter. As we aim to design a converter for portable applications, we want the input voltage to be tens of volts so that it can be readily powered by a battery. For that reason, here we set the input voltage to 45 V.

This material is based upon work supported by the National Science Foundation under Grant No. 1808489.

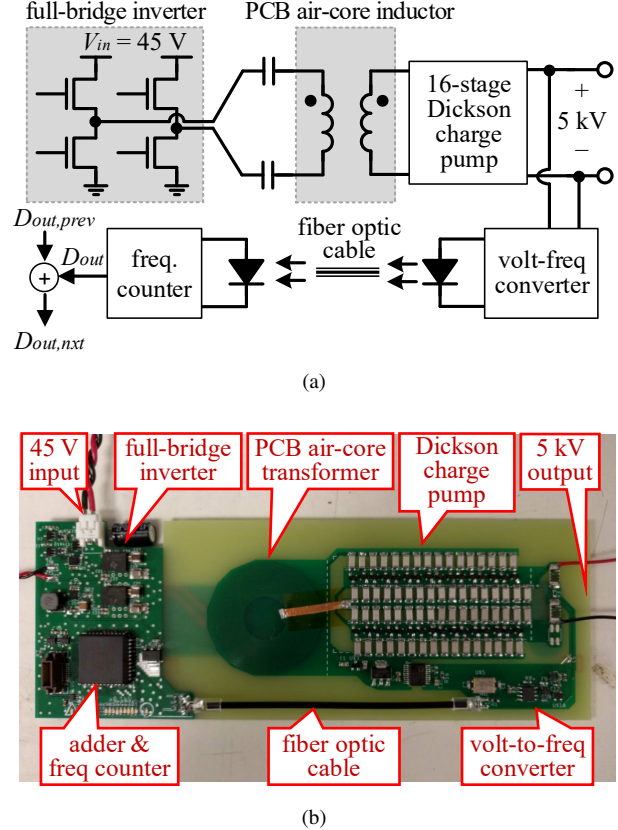


Fig. 1. The developed 100 W 45 V-to-5 kV dc-dc converter. (a) Schematic. (b) Implementation. The photography is taken before the high-voltage side is covered with insulating compound. The circuit board measures 185 mm × 66 mm.

We choose to use a Dickson voltage multiplier for its lower output voltage drop compared to Cockcroft-Walton multiplier [4]. Dickson topology requires coupling capacitors that can withstand half of the output voltage. We find that 3 kV-rated capacitors with C0G dielectric in a small package are readily available. Therefore, the output voltage of individual module is set to 5 kV, derating 6 kV limit with 1 kV safety margin.

2) *Inverter*: A full-bridge inverter switching at 3-7 MHz delivers a 90 V peak-to-peak square wave to a PCB planar air-core transformer. We used a pair of integrated GaN half-

bridge module (LMG5200, Texas Instruments). The leakage inductance of the transformer is used to achieve zero-voltage switching (ZVS). The switching frequency of choice depends on the load condition, as we intend to use frequency control for output voltage regulation. For instance, 3.5 MHz is for 5 kV and 100 W output. The frequency is adjusted to 5.2 MHz when the output is 5 kV and 50 W.

3) *Voltage Multiplier*: For high-frequency voltage rectification and multiplication, we need high-voltage Schottky diode. Moreover, in order to reduce the power loss at the transformer, we need to decrease the amount of charge circulating in and out of the voltage multiplier, which can be achieved by selecting a diode with small parasitic capacitance. At the time of the design, BAT240 (240 V Si Schottky diode) from Infineon Technologies was the most suitable device that meets those criteria.

To further decrease the diode parasitic capacitance by half, we connect two 240 V diodes in series and use it as a single rectifying device. This is easily done since the BAT240 part comes with two diodes already connected in series and integrated in a single SOT23 package. Also, by connecting two diodes in series, the maximum reverse voltage is increased by roughly a factor of two, with some derating to account for mismatch in the reverse characteristics of two diodes [5].

We use a 16-stage Dickson charge pump to rectify the ac voltage at the transformer secondary side and boost up the voltage by a factor of 16. The number of multiplier stages is chosen to be 16 because, for 5 kV dc output voltage, rectifying devices at each multiplier stage (two 240 V diodes connected in series) can comfortably withstand 313 V.

4) *Transformer*: The transformer design is described in Fig. 2. The secondary side of the PCB transformer (top layer of the PCB) picks up the ac voltage of approximately 300 V peak-to-peak. This ac voltage drives a 16-stage Dickson charge pump that generates 5 kV dc at the converter output. As described in the figure, the outer-most turn of the secondary side is tapped and connected to a half-wave rectifier so that a small fraction of the secondary side voltage is used as the supply voltage of the auxiliary circuit on the high-voltage side.

The transformer design begins with the available board space. We first set the width of the circuit board to 66 mm (2.6 inches) and determine the outer diameter of the transformer to be 37 mm by giving a 15 mm clearance from the ground plane and edges of the circuit board. This clearance is to assure high-voltage insulation between the low-voltage side (inverter and the transformer primary side) and the high-voltage side (transformer secondary side). In general, the larger size of the transformer (larger outer diameter) is expected to result in a smaller power loss, but this comes at a cost, namely, larger overall size of the converter.

Next, we determine the inner diameter of the planar transformer to be 12 mm by setting the outer-to-inner diameter ratio to 0.32. This ratio is because the modified Wheeler formula in [6] suggests that the ratio of 0.323 achieves the highest quality factor for a planar spiral inductor, when the turn numbers and the outer diameter are assumed to be fixed. (The detailed

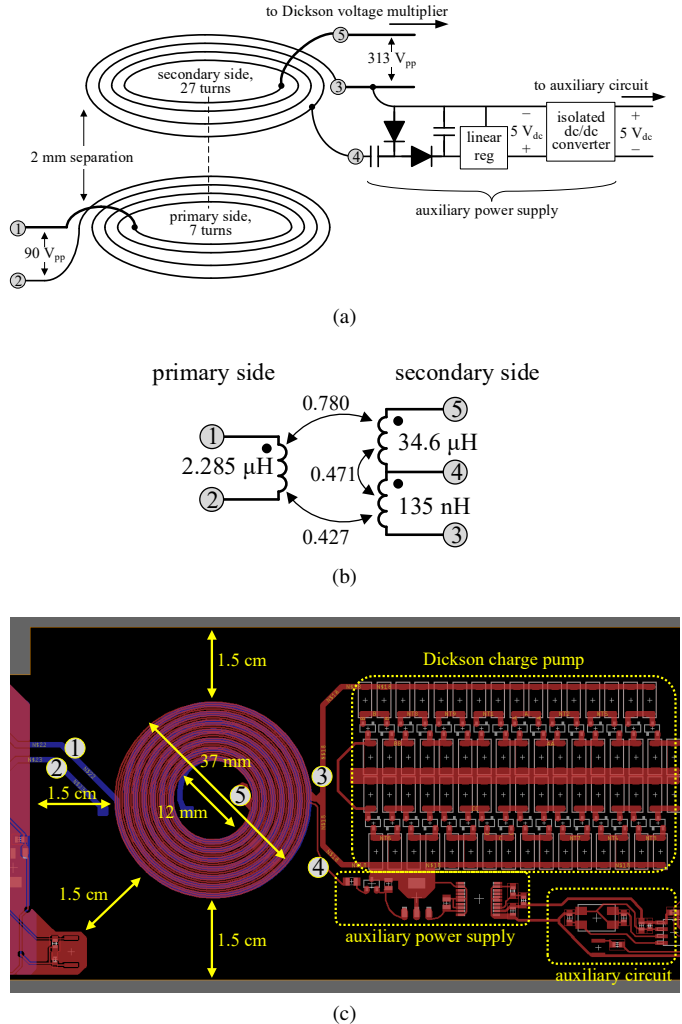


Fig. 2. Description of the PCB spiral transformer. (a) Illustrative diagram. (b) Equivalent circuit model. (c) PCB layout.

derivation will be provided in the upcoming publication that expands this work.)

Then, we pack as many traces as possible onto the available space for the transformer secondary side. The manufacturer we chose requires 6 mil minimum trace width and 6 mil trace-to-trace clearance. Unfortunately, when we tested the transformer with 6 mil-wide traces, manufactured by two different board houses, the series resistance was almost three times lower than expected from the simulation by FastHenry and FEMM. In a few extreme cases, some of the transformers had its trace disconnected in the middle. To compromise with the manufacturing capability of board houses, we increased the trace width to 10 mil. The result is 27 turns of 10 mil-wide secondary-side traces packed in the circular space between 37 mm outer diameter and 12 mm inner diameter circles.

The vertical separation between primary and secondary side is 2 mm, the same as the thickness of the FR4 circuit board. [7] indicates that the FR4 material's breakdown voltage is 800 V/mil, or roughly 30 kV/mm. We use 2 mm-thick board so that the transformer does not experience electric breakdown

through the board for the voltage up to 60 kV.

Finally, we design the primary side to have 7 turns. We set our design goal to achieve 45 V-to-5 kV dc-dc conversion for a single module. Since we set the number of voltage multiplier stages to 16, dividing 5 kV by 16, we find the necessary peak-to-peak voltage at the voltage multiplier input to be 313 V. By running simulations with LTspice and FastHenry, we find that the primary-side turn numbers should be 7 to convert 90 V peak-to-peak square wave at the transformer primary side to 313 V peak-to-peak sine wave at the secondary side.

The copper thickness of the transformer traces is 1 oz/ft² (1.4 mil or 36 μm). A lower resistance and hence lower power loss can be obtained by using a thicker copper such as 2 oz (2.8 mil) or 4 oz (5.6 mil), all readily available at additional cost. Unfortunately, circuit board manufacturers usually require larger clearance between traces when thicker copper is used, which results in lower inductance that forces the converter to operate at higher frequency. This higher frequency exacerbates the skin effect and gives rise to higher power loss, diminishing the benefit of thicker copper traces. Also, the extra cost charged for thicker-copper board was often prohibitive and made it hard to prototype and iterate the design. Therefore, we settled with the 1 oz copper design with densely packed traces for this project.

5) Advantages of the Proposed Design: Followings summarize advantages of the presented circuit design. First, the 54 kV converter comprises 10 modules of 5 kV converters. This modular design allows quick identification and replacement of a malfunctioning part in case of a circuit failure. It is also easy to change the number of cascaded converters for different voltage and power requirements. Second, high-frequency switching at the inverter allows the use of a planar air core transformer, which greatly simplifies the high-voltage isolation between primary and secondary sides. In the presented design, two 37 mm-diameter spiral windings are separated by 2 mm-thick FR4 PCB (primary side on the bottom layer, secondary on the top layer), which is capable of withstanding up to 60 kV dc. Third, a Dickson charge pump is used instead of conventional Cockcroft-Walton for voltage multiplication, which allows smaller coupling capacitors and higher number of multiplier stages. Lastly, two diodes in series work as a single rectifying device in the Dickson charge pump, leading to lower junction capacitance and hence lower circulating current at the transformer. This lower current reduces the copper loss at the transformer which is the major source of power loss in this converter.

B. High-Voltage Insulation and Thermal Management

For electrical insulation and thermal management, the isolated high-voltage side of the converter is covered with 4 mm-thick potting compound. A plastic frame is attached on the circuit board (Fig. 3a), then potting compound is poured into the frame to completely seal the high-voltage side (Fig. 3). The potting compound we used (832TC from MG Chemicals) has a rated breakdown voltage of 46 kV at 3.1 mm layer thickness. Since all components on the high-voltage side has vertical

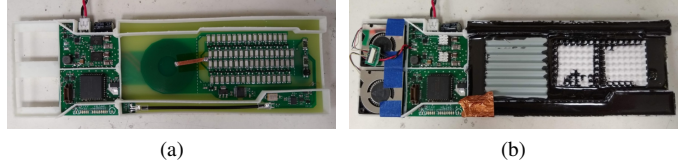


Fig. 3. Electrical insulation and thermal design using a potting frame, heat sinks, potting compound, and fans. (a) Circuit board with the potting frame attached. (b) Finished design with potting compound, ceramic heat sinks, and fans.

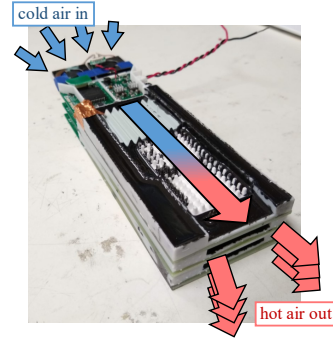


Fig. 4. The airflow through heat sinks when converters are vertically stacked.

dimension of 1 mm or less, we conclude that 4 mm thick layer we use will provide electrical insulation that is higher than 50 kV.

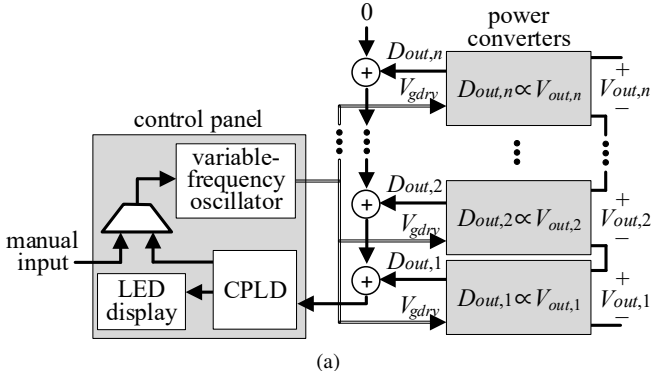
Two cooling fans are installed and 4 mm channel for airflow is provided between modules. Fig. 4 illustrates the airflow between circuit boards and through heat sinks when converter modules are stacked vertically. Due to this structure, it is expected that modules in the middle perform just as well as when it is operated alone.

C. Variable-Frequency Control

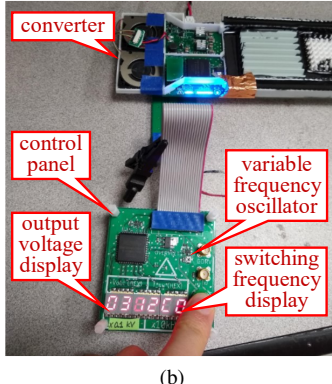
To implement variable frequency control, an optical transmitter based on a voltage-to-frequency converter is installed at the output terminal. A frequency counter converts the optical signal to a digital representation (D_{out}), which then is added to the accumulated output voltage of previous stages ($D_{out,prev}$). The added result ($D_{out,nxt}$) is sent to either the next converter stage or the control panel.

As described in Fig. 5, digital signals $D_{out,1}, \dots, D_{out,n}$ proportional to output voltages $V_{out,1}, \dots, V_{out,n}$ are accumulated and sent to a control panel. A CPLD chip on the control panel reads the digital signal and shows the number on the LED display. The CPLD can be programmed such that it adjusts the inverter switching frequency of power converters via a variable-frequency oscillator, thereby completing the closed-loop feedback. Since the feedback is not implemented in this work, the test shown in Fig. 5b is conducted by manually adjusting the switching frequency to set the output voltage to a desired value.

The oscillator clock signal directly governs the switching events of the bottom-most module. The module then buffers



(a)



(b)

Fig. 5. Variable-frequency control implementation. (a) Schematic. (b) Photograph. The voltage display (hexadecimal; scaling factor $\times 0.1$ kV) and the switching frequency display (hexadecimal; scaling factor $\times 5$ kHz) indicate 4.9 kV and 3.52 kHz, respectively.

the clock signal and pass it on to the next module, which subsequently buffers it and pass it on to the next module, all the way up to the top module. Therefore, one adjusts the switching frequency of all the stacked modules simultaneously by changing the clock frequency at the control panel.

III. EXPERIMENTAL RESULTS

A. A 45 V-to-5 kV Single Module Test

Fig. 6 shows the experimental setup. The input power supply provides a 45 V dc input to the converter under test, which generates a 5 kV dc output to drive the $250\text{ k}\Omega$ load resistor. A multimeter, an oscilloscope, and a thermal camera are used to measure electrical and thermal performances. Fig. 7a shows voltage waveforms of inverter ac outputs and the converter high-voltage dc output. Waveforms indicate that the inverter switches at 3.53 MHz and achieves zero-voltage switching and the converter delivers 5 kV output to the 100 W load. When the load was replaced by a 50 W load in another experiment (Fig. 7b), 5 kV output was maintained by adjusting the inverter switching frequency to 5.19 MHz, demonstrating the ability for variable frequency control. Fig. 8 is a thermal image of the converter taken after 5 minutes of continuous 100 W power delivery to show the converter's thermal performance.

Table I summarizes experimental results. The efficiency is 76.9 % and the total input power is 132.6 W. The standby power, which is the power consumption by the digital circuit,

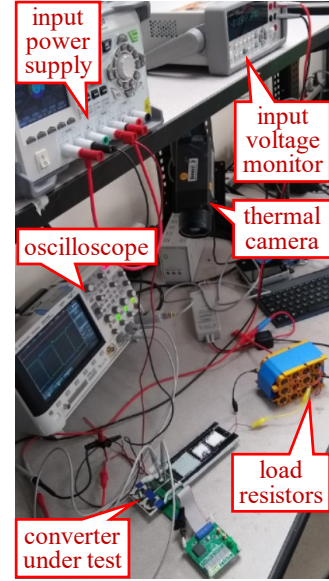
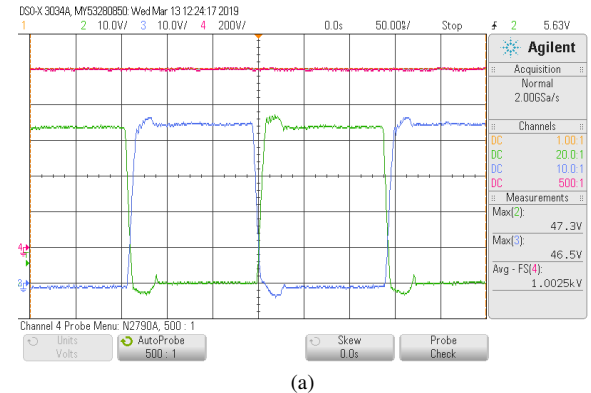
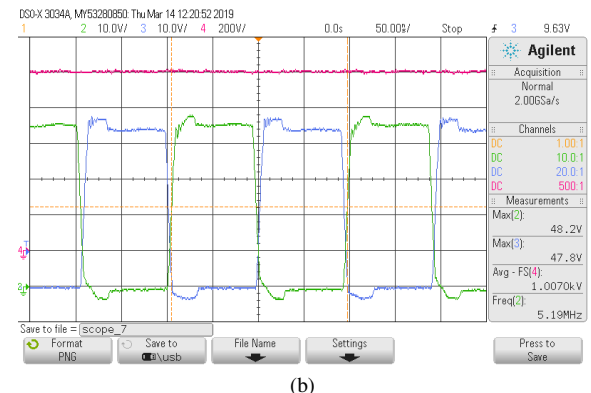


Fig. 6. Experimental setup. The safety cage around the converter was removed for a clear view.



(a)



(b)

Fig. 7. Full-bridge inverter output voltages (green and blue curves; 10 V/div) and the converter output voltage (pink curve; 200 V/div with a 5:1 voltage divider in use). (a) Measured at 5 kV, 100 W dc output. (b) Measured at 5 kV, 50 W dc output.

TABLE I
PERFORMANCE TEST RESULTS OF A 45 V-TO-5 KV CONVERTER.

P_{in}	$P_{in,stby}$	P_{out}	η	η_{pwr}	V_{in}	V_{out}	dimension	in-out isolation
132.6 W	4.3 W	102 W	76.9 %	79.5 %	45 V	5.05 kV	217 × 66 × 10 mm ³	> 55 kV

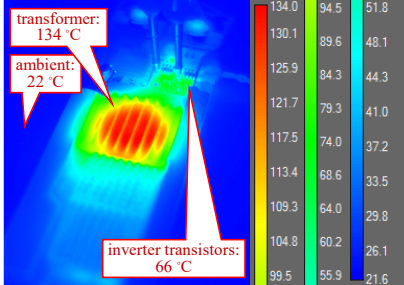
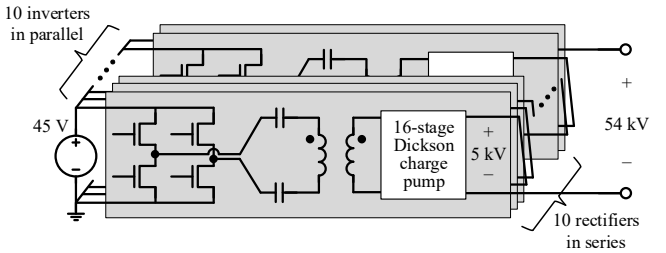


Fig. 8. Thermal image after the converter delivers 5 kV, 100 W output continuously for 5 minutes. Temperature ratings of the potting compound and inverter transistors are 175 °C and 125 °C, respectively, both of which are far above measured temperatures.



(a)



(b)

Fig. 10. Ten converters connected in input-parallel output-series configuration to achieve 45 V-to-54 kV dc-dc power conversion. (a) Illustrative diagram. (b) Photograph.

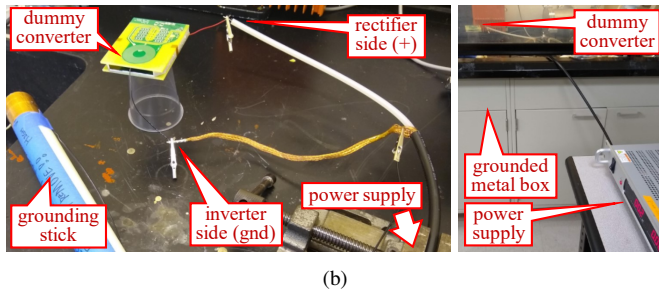


Fig. 9. The hipot test setup to measure the input-to-output isolation breakdown voltage. (a) Schematic. (b) Photographs.

the oscillator, fans, and indicator LEDs, is 4.3 W. Excluding the standby power and only considering the power drawn at the inverter input, the efficiency of power processing circuits is 79.5 %.

B. Insulation Breakdown Voltage Measurement

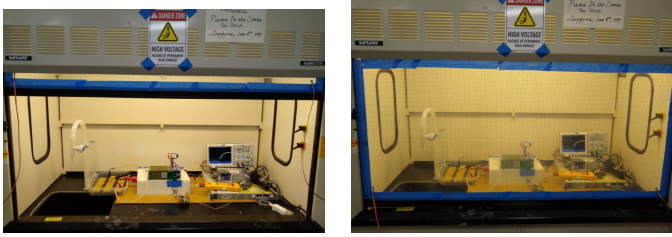
Fig. 9 shows the hipot test setup to measure the input-to-output isolation breakdown voltage. We make a dummy board that replicates the functional converter's electrical insulation, with the high-voltage side partially populated. The breakdown voltage is 55 kV, a promising result for the input-parallel output-series configuration spanning from -50 kV to +50 kV

output. The converter box volume is 0.143 dm³ (8.74 in³), achieving the power density of 713 W/dm³ (11.7 W/in³).

C. 45 V-to-54 kV Multi-Modular Converter Test

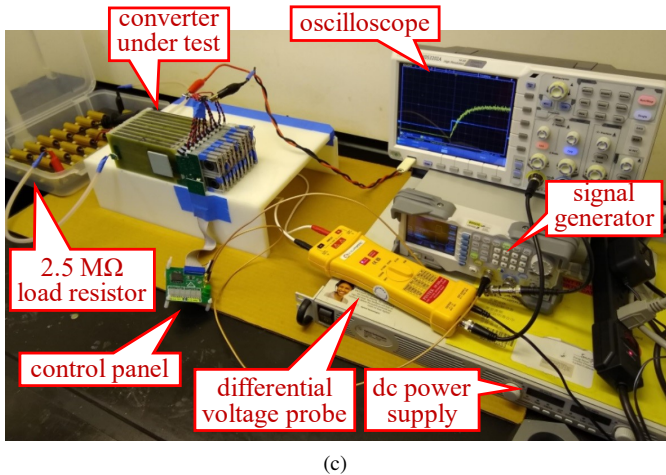
As shown in Fig. 10, we build ten identical converter modules and cascade them so that they are connected to each other in input-parallel output-series manner. Fig. 10a is the schematic diagram and Fig. 10b is the photograph of the converter under test.

Fig. 11 shows the experimental setup. To protect ourselves from high voltage, we installed the setup on a bench enclosed by an earth-grounded metal box. We then put a grounded steel wire mesh on the screen door so that the setup is completely encapsulated when the door is closed. Additionally, we powered all our electric equipment via outlets installed on the metal box so that they share the earth node with the metal box. Also, those outlets are equipped with ground-fault circuit interrupter for extra safety. The high-voltage converter was tested only when the screen door is closed. As shown in Fig. 11c and 11d, we use a 2.5 MΩ resistor for 54 kV dc voltage, which translates to 1166 W total power, or 116.6 W for each 5 kV module. The load resistor doubles as a 50:1 resistive divider, reducing the voltage to 1.1 kV so that it can be measured with a differential voltage probe we have.

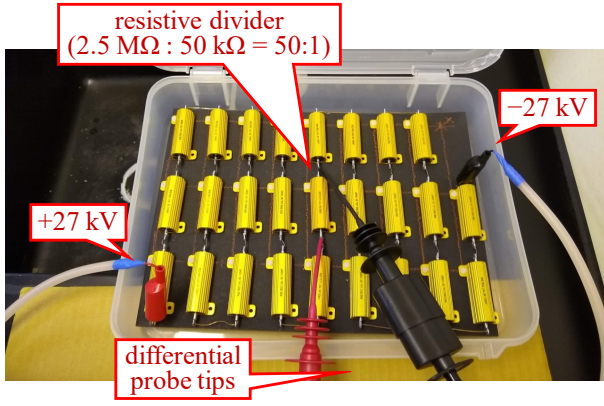


(a)

(b)



(c)

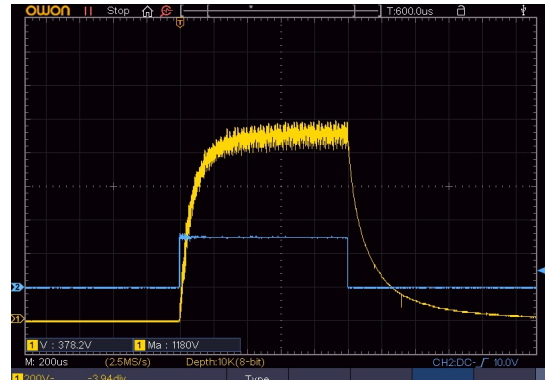


(d)

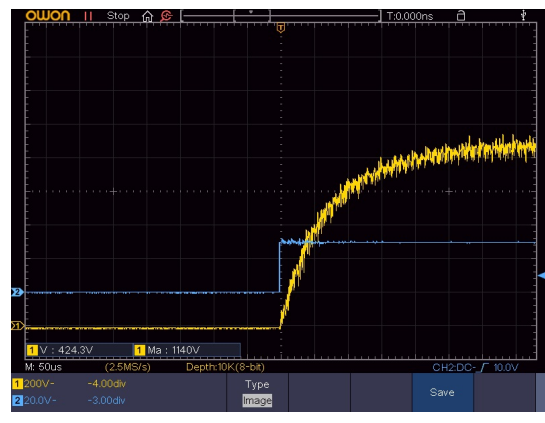
Fig. 11. Experimental setup on a workbench enclosed by an earth-grounded metal box. (a) Bench with the wire mesh door opened. (b) Bench with the wire mesh door closed. (c) Close-up photo of the setup. (d) Close-up photo of the load resistor, which doubles as a 50:1 resistive divider for output voltage measurement.

Fig. 12 shows the measured output voltage of the converter, transitioning from zero to 54 kV and then back to zero after 1 ms. The ripple on the waveform is due to the electromagnetic noise picked up by the long lead wire between the differential voltage probe tip and the body. To confirm the cause of this ripple, we shorted the probe tips in another experiment and observed the same noise being picked up even when ideally the probe should read flat zero voltage.

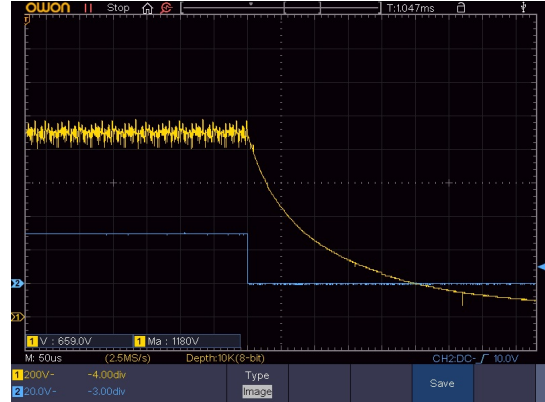
Fig. 13 summarizes the experimental results. As can be



(a)

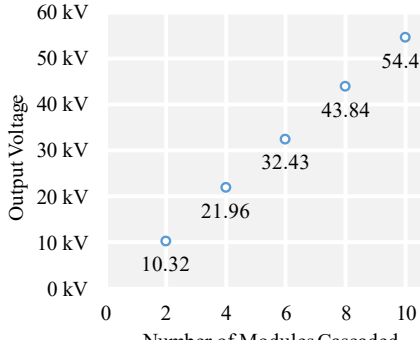


(b)

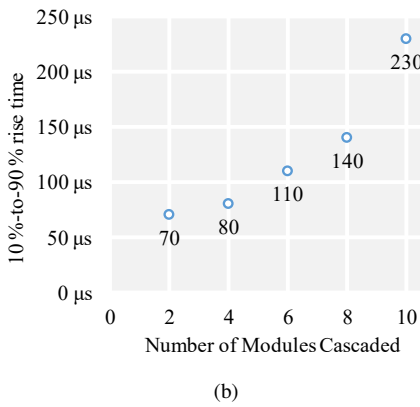


(c)

Fig. 12. Measured waveforms of the high-voltage output (yellow curve, 10 kV/div) and the on-off control signal (blue curve, 2 V/div). We pulse the output for 1 ms to observe the transient speed (timescale 200 μs/div). (a) The entire pulse shape. (b) Close-up of the turn-on transient. (c) Close-up of the turn-off transient.



(a)



(b)

Fig. 13. Plots summarizing the experimental results. (a) Output voltage vs. number of modules cascaded. (b) Rise time vs. number of modules cascaded.

seen in Fig. 13a, the output voltage linearly increases with the number of cascaded modules, which is the result we expected. Fig. 13b shows that the rise time of the converter increases, perhaps quadratically, with the number of modules. This can be explained as the intrinsic rise time of the dc-dc converter module, added with the rise time caused by the parasitic capacitance between the high-voltage side of the converter with the ground node, particularly between transformer primary and secondary sides. This result implies that in order to achieve sub-100 μ s rise time as required by pulsing applications such as pulsed-CT scanners [8], it is necessary to reduce the parasitic capacitance between two sides of the transformer.

IV. CONCLUSION

This paper presented the design and experimental results of a 5 kV isolated dc-dc converter. Design choices that led to a high power density were described, and the performance was experimentally evaluated. Fig. 14 is the power density survey of commercial high-voltage power supplies from various manufacturers. Owing to the modular design, the single module power density (marked with an orange star) remains unchanged for the ten-module 54 kV converter (marked with a blue star), which is a vast improvement over conventional high-voltage dc generation technology.

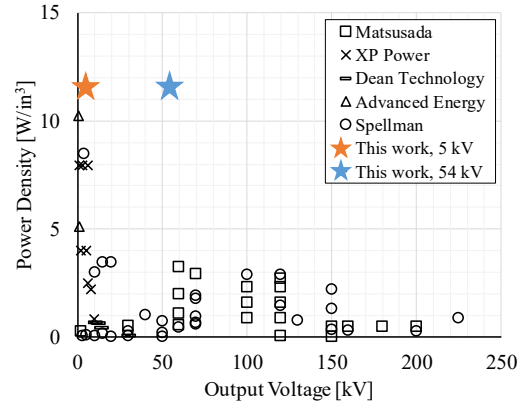


Fig. 14. Power density comparison with some of the commercial high-voltage dc-dc converters. The survey is not exhaustive as the purpose here is to illustrate the status of current technologies.

ACKNOWLEDGMENT

This material is based upon work supported by the National Science Foundation under Grant No. 1808489.

REFERENCES

- [1] G. Zentai, "X-ray imaging for homeland security," in *2008 IEEE International Workshop on Imaging Systems and Techniques*. IEEE, 2008, pp. 1–6.
- [2] W. R. Arnold, "Neutron generating apparatus," Mar. 19 1963, US Patent 3,082,326.
- [3] J. L. Jones, D. R. Norman, K. J. Haskell, J. W. Sterbentz, W. Y. Yoon, S. M. Watson, J. T. Johnson, J. M. Zabriskie, B. D. Bennett, R. W. Watson *et al.*, "Detection of shielded nuclear material in a cargo container," *Nuclear Instruments and Methods in Physics Research Section A: Accelerators, Spectrometers, Detectors and Associated Equipment*, vol. 562, no. 2, pp. 1085–1088, 2006.
- [4] J. F. Dickson, "On-chip high-voltage generation in mnos integrated circuits using an improved voltage multiplier technique," *IEEE Journal of solid-state circuits*, vol. 11, no. 3, pp. 374–378, 1976.
- [5] S. Park, G. Zulauf, and J. Rivas-Davila, "Estimating the reliability of series-connected schottky diodes for high-frequency rectification," in *2018 IEEE 19th Workshop on Control and Modeling for Power Electronics (COMPEL)*. IEEE, 2018, pp. 1–9.
- [6] S. S. Mohan, M. del Mar Hershenson, S. P. Boyd, and T. H. Lee, "Simple accurate expressions for planar spiral inductances," *IEEE Journal of Solid-State Circuits*, vol. 34, no. 10, pp. 1419–1424, Oct 1999.
- [7] R. Tarzwell and K. Bahl, *High Voltage Printed Circuit Design and Manufacturing Notebook*. SIERRA Proto Express, 2004.
- [8] U. Wiedmann, V. B. Neculaes, D. Harrison, E. Asma, P. E. Kinahan, and B. De Man, "X-ray pulsing methods for reduced-dose computed tomography in pet/ct attenuation correction," in *Medical Imaging 2014: Physics of Medical Imaging*, vol. 9033. International Society for Optics and Photonics, 2014, p. 90332Z.